Supporting Information

Ultrafast and high-resolution X-ray imaging based on zero-dimensional organic silver halides

Yongqiang Zhou[a], Zixian Wang[a], linfeng Guo[a], Lei Huang[a], Yichen Liu[a], Mengyue Wu[a], Qian Zhang[a], Kang An[b], Peng He[b], Fei Wang[d], Juan Du[e,f], Zhengzheng Liu[e], Zhiping Hu[f], Yayun Pu[a,*], Jun'an Lai[b,*], Xiaosheng Tang[a,b,c,*]

[a] College of Optoelectronic Engineering, Chongqing University of Posts and Telecommunications, Chongqing, 400065, China.

[b] Key Laboratory of Optoelectronic Technology & Systems (Ministry of Education), College of Optoelectronic Engineering, Chongqing University, Chongqing 400044, China.

[c] School of Materials Science and Engineering, Zhengzhou University, Zhengzhou 450001, China.

[d] College of Materials Science and Engineering, Sichuan University, Chengdu 610065, China.

[e] State Key Laboratory of High Field Laser Physics and CAS Center for Excellence in Ultra-intense Laser Science, Shanghai Institute of Optics and Fine Mechanics, Chinese Academy of Sciences, 201800 Shanghai, China.

[f] School of Physics and Optoelectronic Engineering, Hangzhou Institute for Advanced Study, University of Chinese Academy of Sciences, 310024 Hangzhou, China.

* Corresponding author

E-mail: **puyy@cqupt.edu.cn (Y.Y. Pu), ja.lai@cqu.edu.cn (J. Lai), xstang@cqu.edu.cn (X.S. Tang)**

Concerned physical relation

The optical bandgap can be calculated by the formula below:[1]

$$(h\nu F(A))^{\frac{1}{n}} = A(h\nu - E_g) \tag{S1}$$

where F(A) is the absorption coefficient, $h\nu$ is the photon energy, A is the proportional constant and E_g is the optical bandgap. n = 1/2 is adopted for the estimations owning to the direct bandgap of TPPAgX$_2$.

Spectral splitting was not found over a wide range of temperature, verifying the single emitting center instead of multiple excited states. Due to the enhanced thermal non radiative recombination, the radiation intensity shows a significant increase at first and then decrease with temperature rises up. The activation energy (E_a) for the activation of PL intensity can be extracted through the Arrhenius formula:[2]

$$I(T) = I_0/(1 + Ae^{\frac{E_a}{k_B T}}) \tag{S2}$$

where I(T) and I_0 represent the emission intensity at individual temperatures (T) and 0 K, respectively, and k_B represents the Boltzmann constant.

As the temperature increases from 80 K to 320 K, the emission linewidth (FWHM) broadened gradually, which resulted from the pronounced exciton–phonon coupling effect. The Huang–Rhys factor (S) based on the following formula:[3]

$$FWHM(T) = 2.36\sqrt{S}\hbar\omega_{phonon}\sqrt{coth(\frac{\hbar\omega_{phonon}}{2K_B T})} \tag{S3}$$

where $\hbar$ is the reduced Planck constant, ω_{phonon} is the frequency of longitudinal optical phonon, and k_B is the Boltzmann constant.
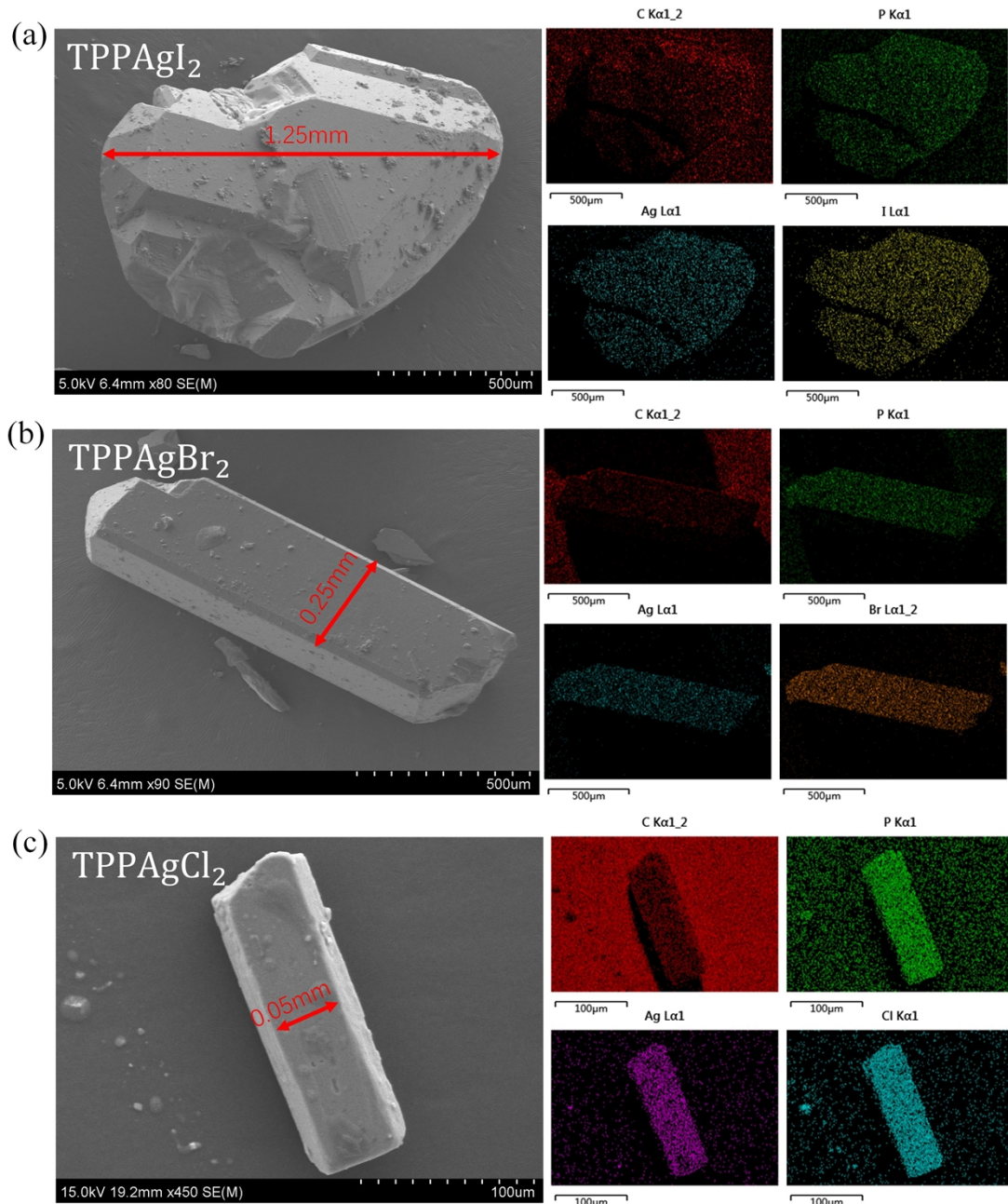
Figure S1. Rod-like crystals of TPPAgX$_2$ (X = I, Br, Cl) and its element distribution analysis by energy dispersive spectroscopy (EDS) mapping. The diameter of the single crystal rod is about 1.25 mm, 0.75 mm, 0.05 mm.
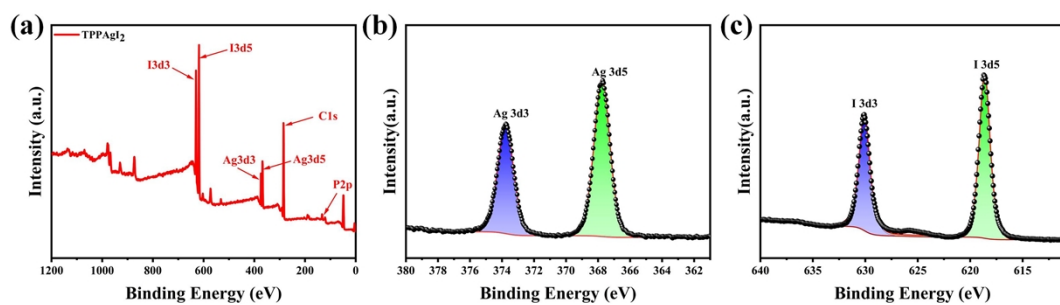
Figure S2. (a) Survey X-ray photoelectron spectrum (XPS) of TPPAgI$_2$. No impurity elements other than TPPI, Ag, and I. High resolution scans of (b) Ag, (c) I. All elements are in the expected valence states.
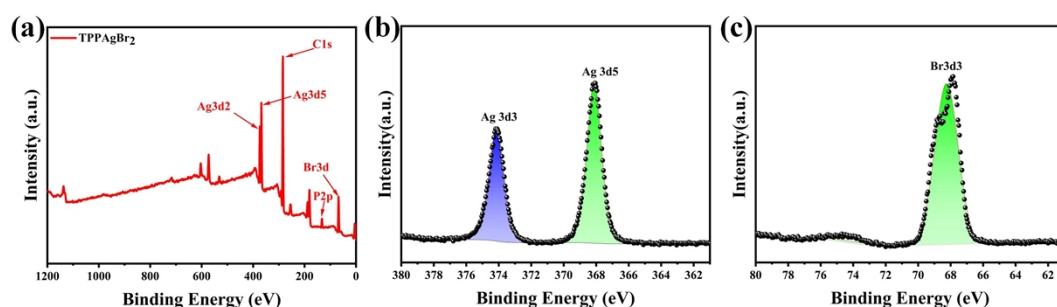
Figure S3. (a) Survey X-ray photoelectron spectrum (XPS) of TPPAgBr$_2$. No impurity elements other than TPPI, Ag, and Br. High resolution scans of (b) Ag, (c) Br. All elements are in the expected valence states.
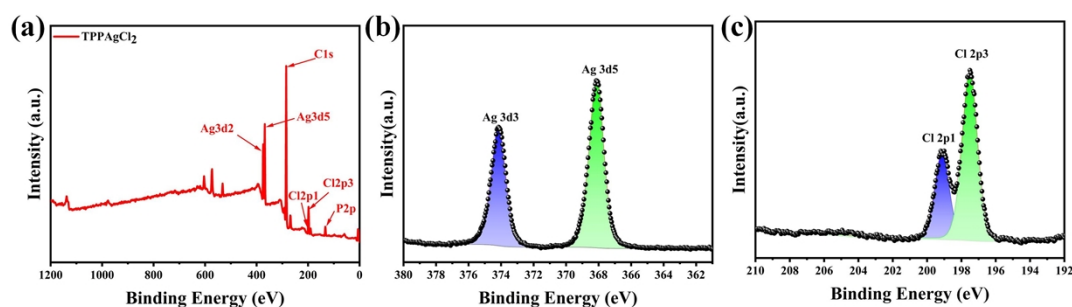

Figure S4. (a) Survey X-ray photoelectron spectrum (XPS) of TPPAgCl$_2$. No impurity elements other than TPPI, Ag, and Cl. High resolution scans of (b) Ag, (c) Cl. All elements are in the expected valence states.
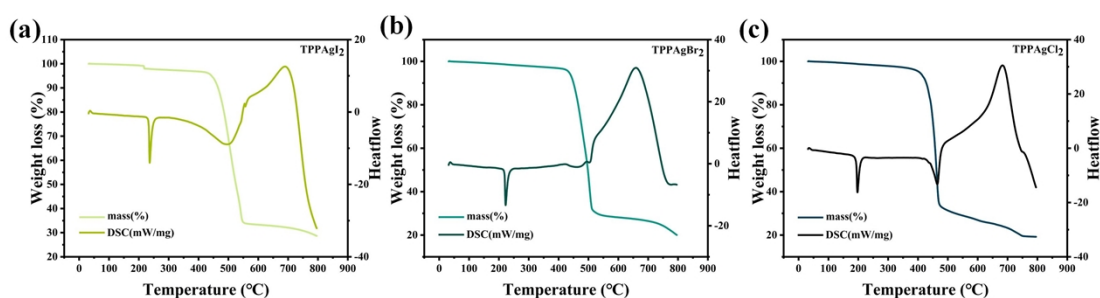


Figure S5. Thermogravimetric analysis (TGA) and differential scanning calorimeter (DSC) analysis of (a) TPPAgI$_2$, (b) TPPAgBr$_2$, (c) TPPAgCl$_2$ powder under N$_2$ flowing atmosphere using a ramp rate of 20°C min^{-1} from 20 to 800°C.
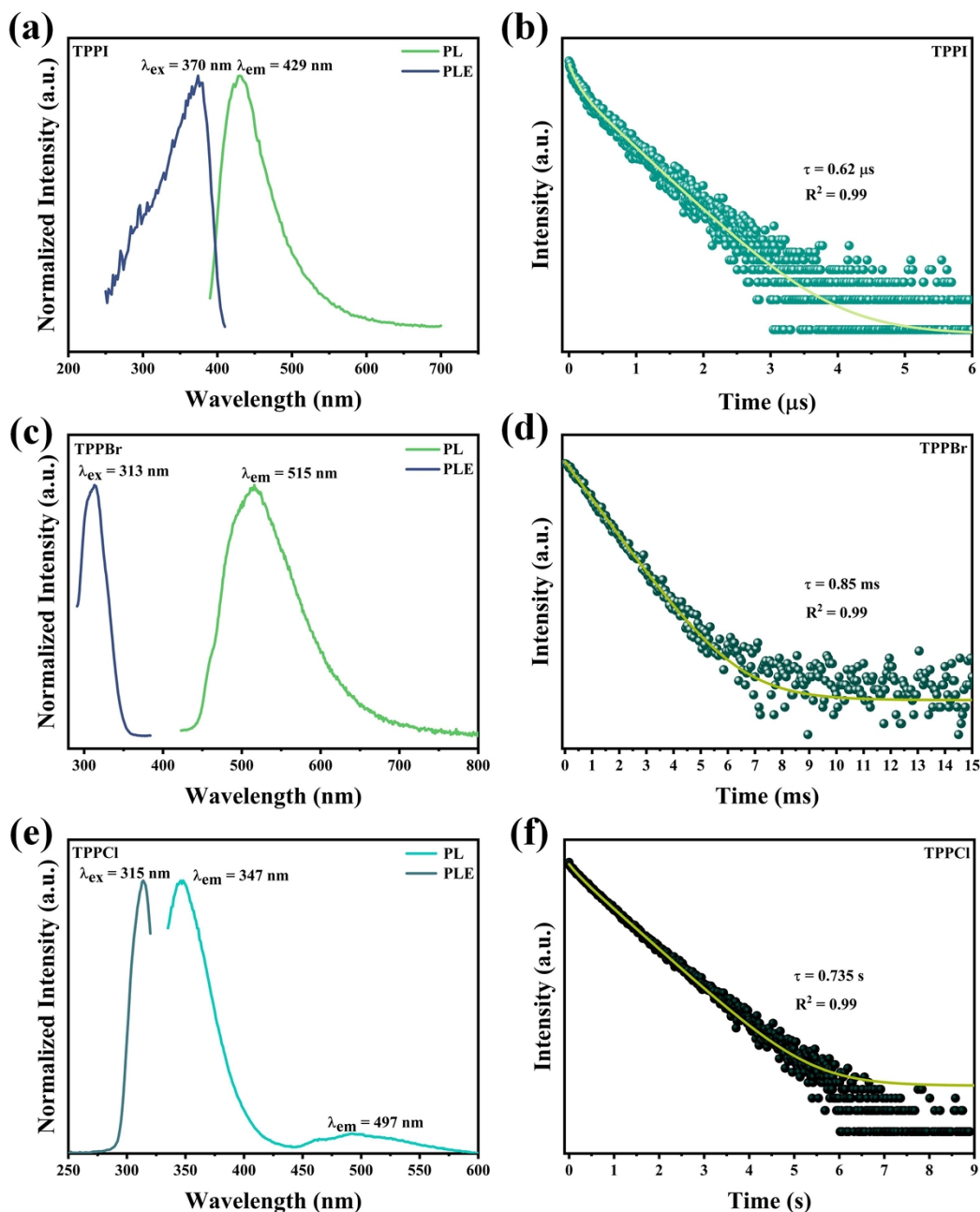
Figure S6. (a, c, e) The normalized excitation spectrum and emission spectrum of TPPI/Br/Cl. (b, d, f) time-resolved PL curve of the TPPI/Br/Cl, the fluorescence lifetime of TPPI is obtained by excitation of 370 nm and emission of 429 nm, TPPBr is obtained by excitation of 313 nm and emission of 515 nm, TPPCl is obtained by excitation at 315 nm and emission at 497 nm.
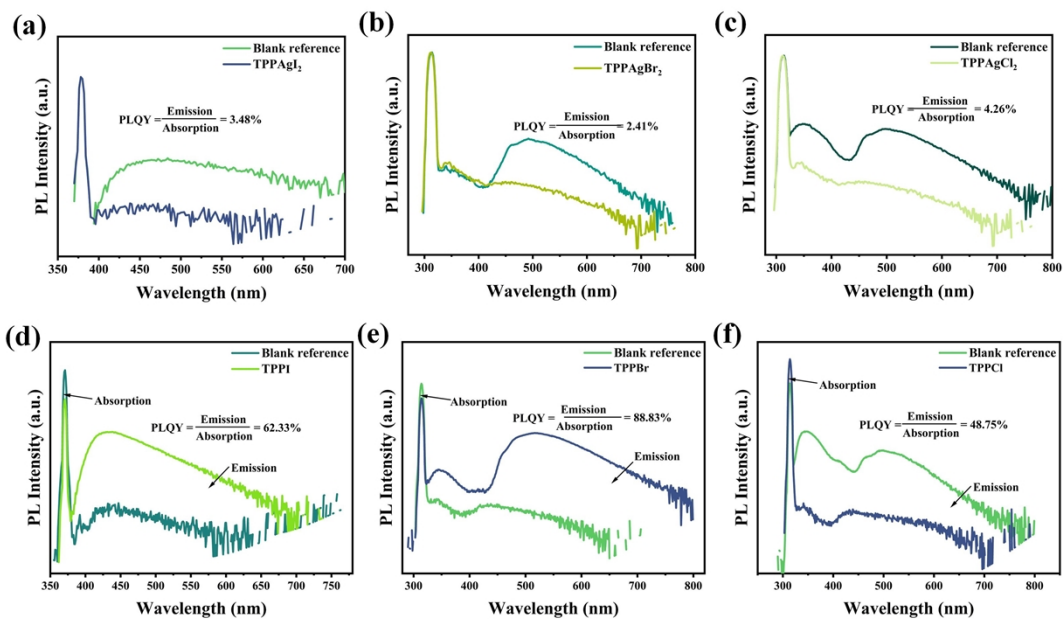
Figure S7. The photoluminescence quantum yield (PLQY) spectra. We placed the TPPAgX$_2$ (X = I, Br, Cl) crystals and TPPI/Br/Cl on a clean quartz plate and tested it in an integrating sphere. The reference is measured by placing a blank quartz plate in the integrating sphere. (a - c) PLQY of TPPAgX$_2$ (X = I, Br, Cl). (d - f) PLQY of TPPI/Br/Cl.
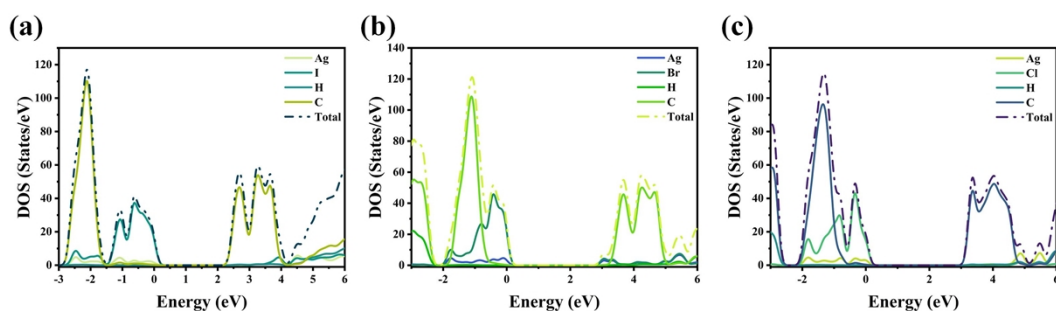

Figure S8. (a) – (c) is the Total and projected density of states (DOS) of the states of TPPAgI$_2$, TPPAgBr$_2$, and TPPAgCl$_2$, respectively.
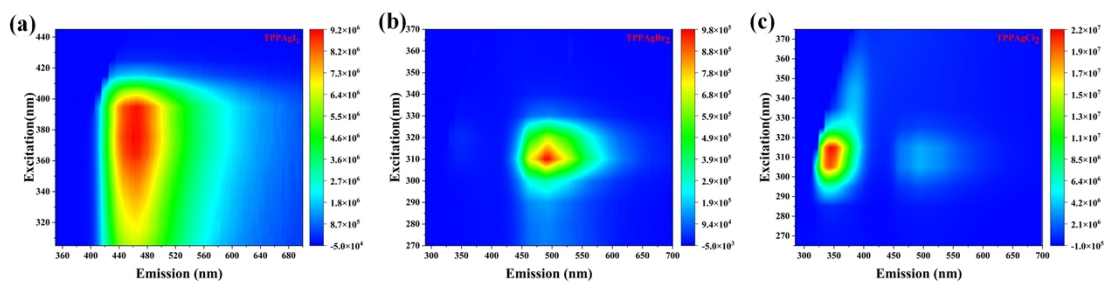

Figure S9. 3D PL excitation and emission correlation map. The correlation between the excitation and emission of (a) TPPAgI$_2$ crystal, with the main excitation around 378
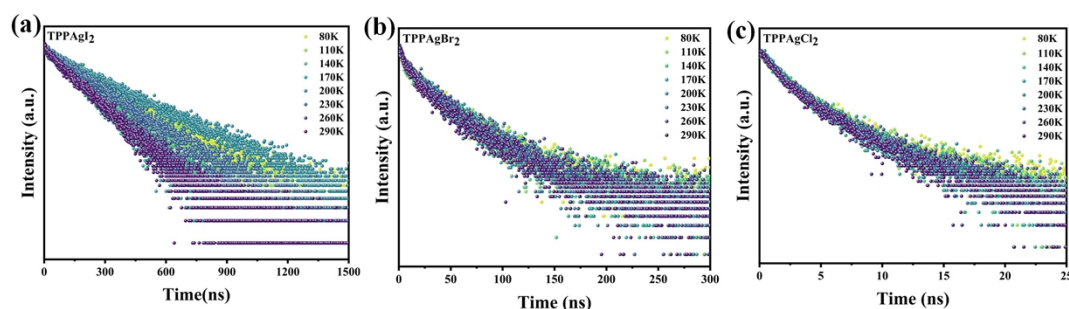
nm and the main emission around 462 nm. (b) TPPAgBr$_2$ crystal, excitation around 316 nm and emission around 492 nm. (c) TPPAgCl$_2$ crystal, excitation around 315 nm and emission around 356 nm.
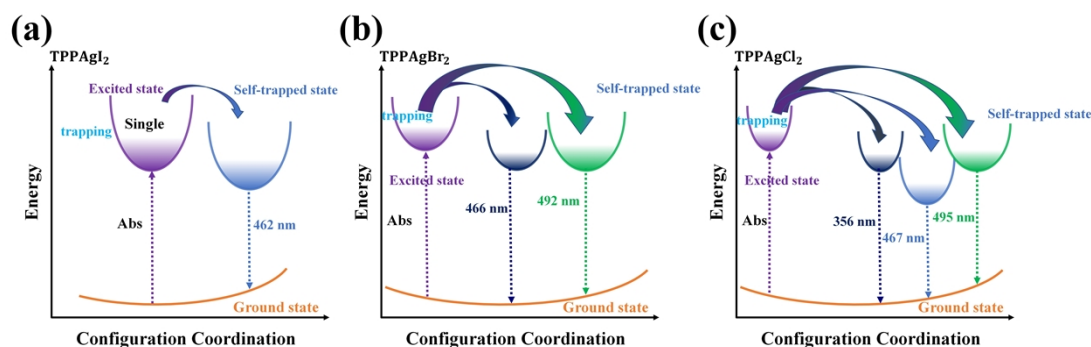
Figure S10. Schematic diagram of the single self-trapped luminescence mechanism of TPPAgX$_2$ (X = I, Br, Cl).
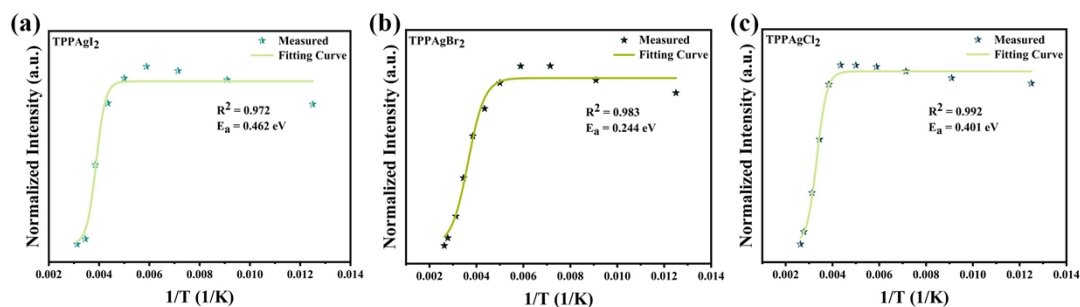
Figure S11. (a - c) Fitting results of PL intensity as a function of temperature.

Figure S12. (a - c) PL decay time diagram of crystal at different temperatures (80 - 290 K). The fluorescence lifetime of TPPAgI$_2$ is obtained by excitation of 378 nm and emission of 462 nm. The fluorescence lifetime of TPPAgBr$_2$ was obtained by excitation of 316 nm and emission of 466 nm. The fluorescence lifetime of TPPAgCl$_2$ was obtained by excitation of 312 nm and emission of 467 nm.

According to the dipole selection rule,[4] the singlet state is first filled under ultraviolet excitation, and then the excitons gradually fill the triplet state through ISC. It can return directly to the ground state by emitting phosphorescence, or it can be emitted TADF via the RISC path. The difference is that under X-ray irradiation, high-energy X-ray photons first interact with heavy atoms through the photoelectric effect and Compton scattering. Subsequently, high-energy internal electrons are ejected and then collide with other atoms, producing a large number of secondary electrons.[5] This process will continue until all the secondary electrons do not have enough energy to ionize or excite other molecules.[6] These low-energy secondary electrons usually play a major role in the electronic transitions that induce luminescence. Thus, similar to the case of electrical excitation, the excitons produced by recombination fill the triplet and singlet states in a ratio of 3:1 according to the spin conservation law.[7] Thus, in scintillation, more X-ray induced triplet excitons can be generated and perform TADF emission.
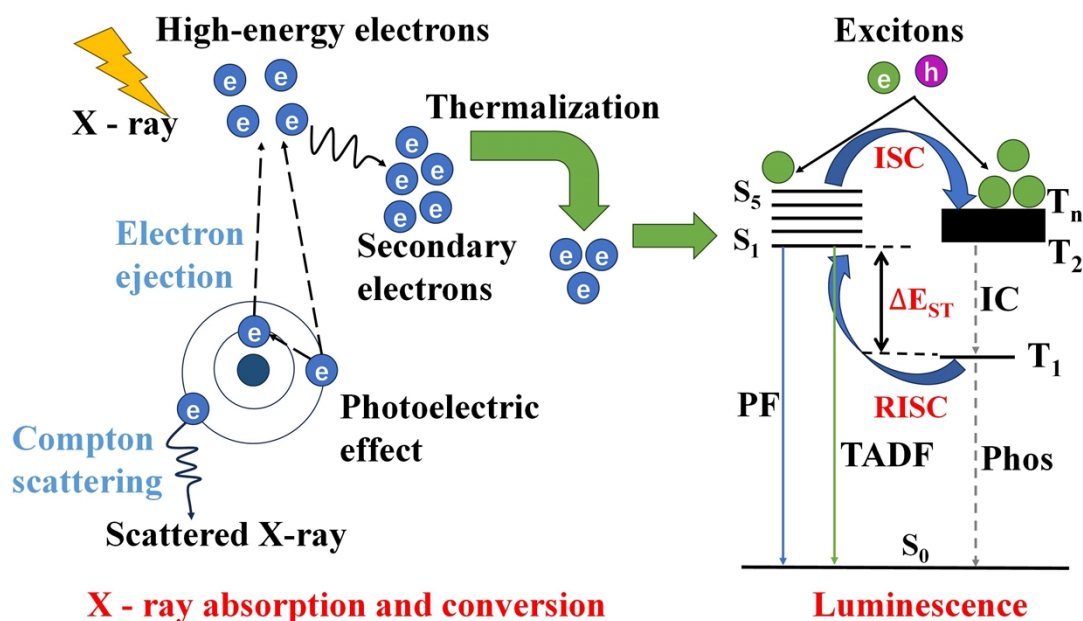
Figure S13. Schematic diagram of luminescence mechanism during the RL process of TPPAgCl$_2$.[8]

(a)

LUMO -4.72 eV

GAP 5.36 eV

HOMO -10.08 eV

(b)

LUMO -2.01 eV

GAP 3.54 eV

HOMO -5.55 eV
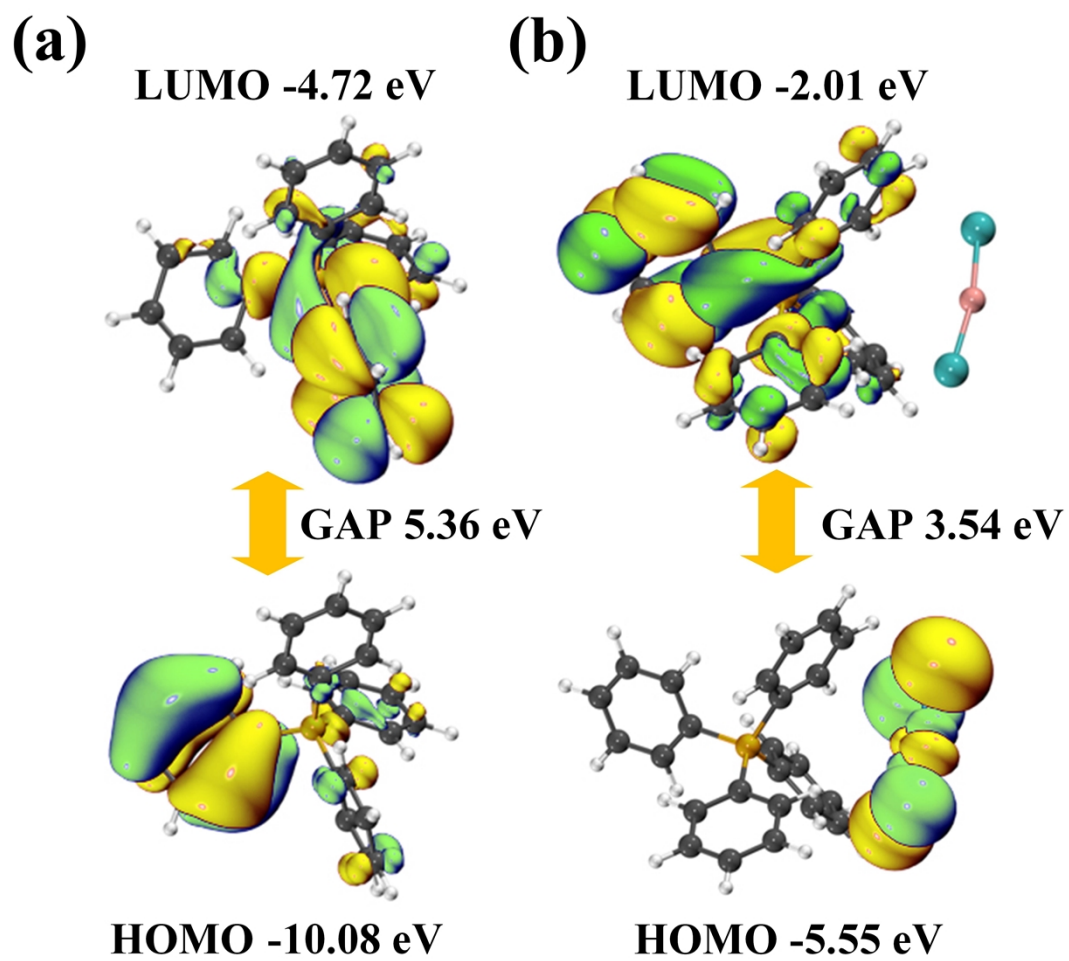
Figure S14. (a) and (b) are the Highest Occupied Molecular Orbit (HOMO) and Lowest Unoccupied Molecular Orbit (LUMO) of TPPCl and TPPAgCl$_2$, respectively.
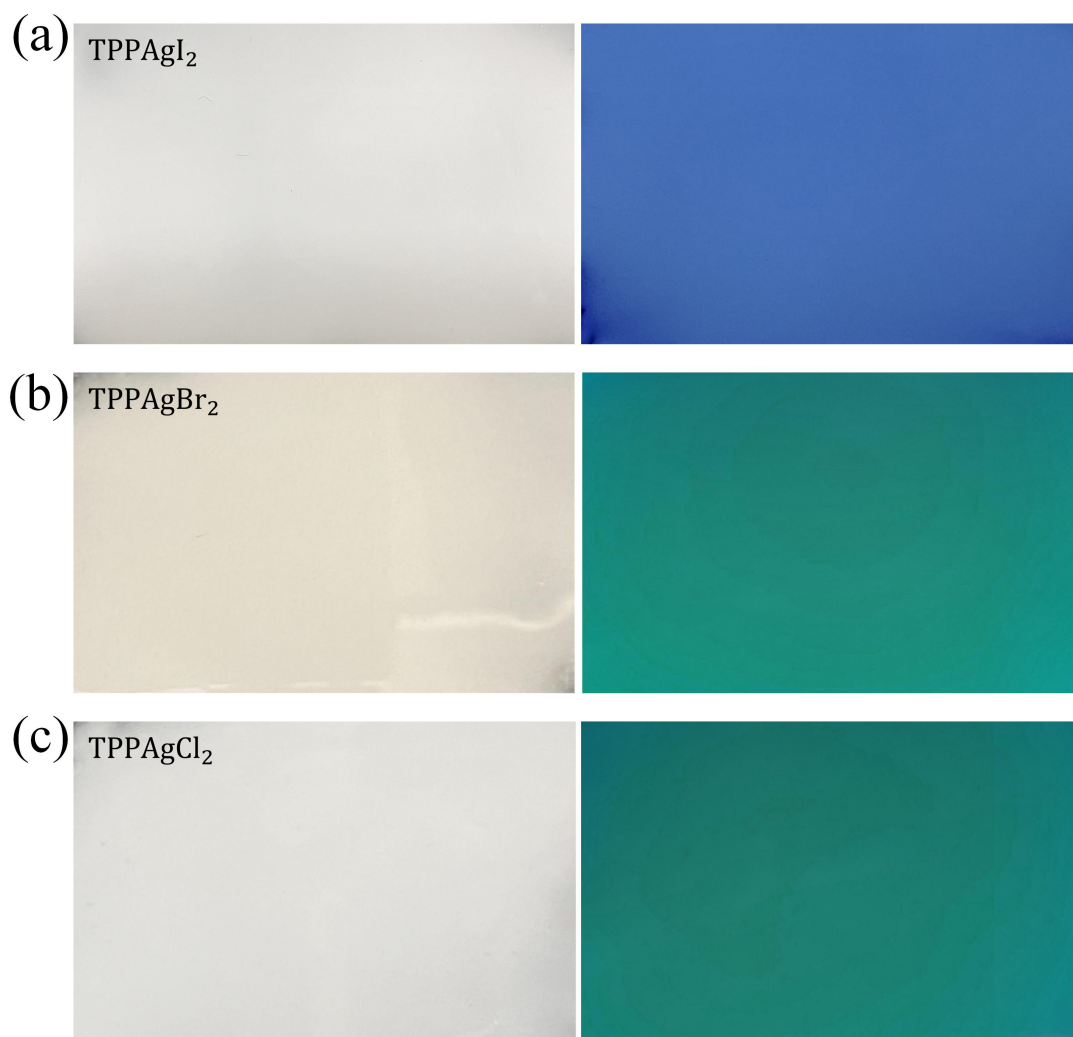
Figure S15. Figures on left show the picture of TPPAgX$_2$ (X = I, Br, Cl) irradiated under visible light, and on the right show the picture irradiated under UV light, where (a) irradiated by 365 nm UV light, (b-c) irradiated by 254 nm UV light.
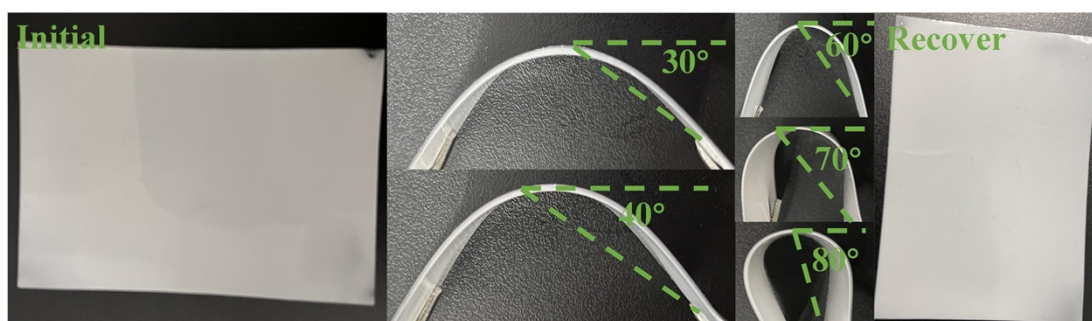
Figure S16. Flexible testing of X-ray imaging films made from a mixture of TPPAgX$_2$ (X = I, Br, Cl) and PDMS (30°-80°).
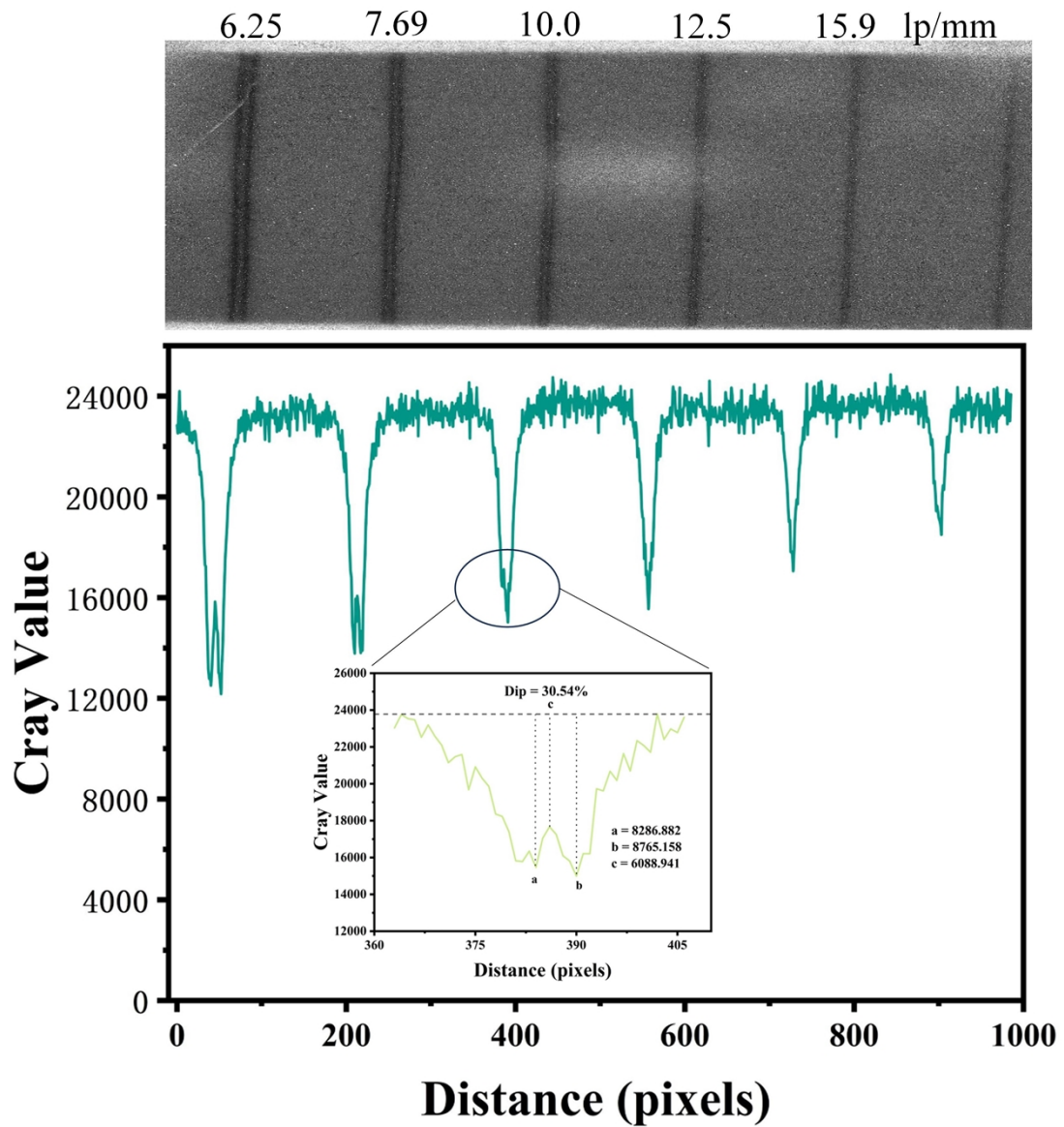
Figure S17. Plot of line pair image analysis at basic spatial resolution obtained by comparison using standard cards.

Table S1. The chemical composition data measured by EDS of TPPAgX$_2$ (X = I, Br, Cl) crystal.

Crystal materials	C	P	Ag	I/Br/Cl	Total
TPPAgI$_2$	51.58%	15.83%	10.67%	21.92%	100%
TPPAgBr$_2$	56.58%	14.47%	18.93%	10.02%	100%
TPPAgCl$_2$	87.39%	3.95%	5.94%	2.72%	100%

Table S2. Single crystal X-ray diffraction data of TPPAgI$_2$ single crystals.

Compound	TPPAgI$_2$
Empirical formula	(C$_{24}$H$_{20}$P)AgI$_2$
Formula weight	1402.08
Temperature/K	200.0
Crystal system	monoclinic
space group	P-1
a/Å	11.0509(5)
c/Å	13.3965(6)
α/°	16.5842(8)
β/°	83.100(2)
γ/°	97.245(2)
γ/°	76.019(2)
Volume/Å^3	2315.72(19)
Z	2
R$_1$, wR$_2$	0.1438(7612), 0.3413(9358)
ρ$_{calc}$g/cm^3	2.011

Table S3. Single crystal X-ray diffraction data of TPPAgBr$_2$ single crystals.

Compound	TPPAgBr$_2$
Empirical formula	(C$_{24}$H$_{20}$P)AgBr$_2$
Formula weight	607.06
Temperature/K	298.0
Crystal system	monoclinic
space group	P12$_1$/n1
a/Å	14.4708(11)
b/Å	7.8856(6)
c/Å	19.9274(15)
α/°	90
β/°	103.067(3)
γ/°	90
Volume/Å^3	2215.1(3)
Z	4
R$_1$, wR$_2$	0.0718(3594), 0.1822(3875)
ρ$_{calc}$g/cm^3	1.820

Table S4. Single crystal X-ray diffraction data of TPPAgCl$_2$ single crystals.

Compound	TPPAgCl$_2$
Empirical formula	(C$_{24}$H$_{20}$P)AgCl$_2$
Formula weight	518.14
Temperature/K	293.0
Crystal system	monoclinic
space group	P121/n1
a/Å	14.2365(6)
b/Å	8.0965(3)
c/Å	19.2365(9)
α/°	90
β/°	101.581(4)
γ/°	90
Volume/Å^3	2172.17(16)
Z	4
R$_1$, wR$_2$	0.0422(3947), 0.1276(5240)
ρ$_{calc}$g/cm^3	1.584

References

1.   Perfetti, Quaresima, Capasso, Capozi, Evangelisti, Boscherini and Patella, Electronic properties of the precrystallization regime of germanium: A photoemission study, *Physical review. B, Condensed matter*, 1986, **33**, 6998-7005.
2.   B. Ai, C. Liu, Z. Deng, J. Wang, J. Han and X. Zhao, Low temperature photoluminescence properties of CsPbBr3 quantum dots embedded in glasses, *Physical Chemistry Chemical Physics*, 2017, **19**, 17349-17355.
3.   D. Y. Li, Y. B. Shang, Q. Liu, H. W. Zhang, X. Y. Zhang, C. Y. Yue and X. W. Lei, 0D hybrid indium halide as a highly efficient X-ray scintillation and ultra-sensitive fluorescent probe, *Mater. Horizons*, 2023, DOI: 10.1039/d3mh00536, 12.
4.   F. D. Brooks, Development of organic scintillators, *Nuclear Instruments and Methods*, 1979, **162**, 477-505.
5.   R. C. Sangster and J. W. Irvine, Jr., Study of Organic Scintillators, *The Journal of Chemical Physics*, 1956, **24**, 670-715.
6.   G. Laustriat, The luminescence decay of organic scintillators, *Molecular Crystals*, 1968, **4**, 127-145.
7.   W. Ma, Y. Su, Q. Zhang, C. Deng, L. Pasquali, W. Zhu, Y. Tian, P. Ran, Z. Chen, G. Yang, G. Liang, T. Liu, H. Zhu, P. Huang, H. Zhong, K. Wang, S. Peng, J. Xia, H. Liu, X. Liu and Y. M. Yang, Thermally activated delayed fluorescence (TADF) organic molecules for efficient X-ray scintillation and imaging, *Nat. Mater.*, 2022, **21**, 210-216.
8.   F. Zhang, Y. Zhou, Z. Chen, M. Wang, Z. Ma, X. Chen, M. Jia, D. Wu, J. Xiao, X. Li, Y. Zhang, Z. Shi and C. Shan, Thermally Activated Delayed Fluorescence Zirconium-Based Perovskites for Large-Area and Ultraflexible X-ray Scintillator Screens, *Adv. Mater.*, 2022, **34**, 2204801.